Synthesis Report
BRE2-0007
JE - 5020

MOLTEN SALT CATALYSTS FOR SULFURIC ACID PRODUCTION AND SO_2 REMOVAL FROM FLUE GAS (MOLTCAT)

S. Boghosian, F. Borup, A. Chrissanthopoulos, D. A. Karydis and G. N. Papatheodorou
Institute of Chemical Engineering and High Temperature Chemical Processes (FORTH-ICE/HT), P.O. Box 1414, GR-26500 Patras GREECE

N. J. Bjerrum, F. Cappeln, K. M. Eriksen, R. Fehrmann, K. Nielsen, S. G. Masters, C. Oehlers and 1. Petrushina
Chemistry Department, Building 207, The Technical University of Denmark, DK-2800 Lyngby, DENMARK

ABSTRACT

The catalytic active centers and the additive effects on catalytic active centers have been studied by spectrophotometric (UV-VIS) and spectroscopic (Raman, NMR) methods at high temperatures for the molten salt-gas system $M_2S_2O_7/MHSO_4/M_2SO_4/V_2O_5$ - S0/0,/$S0_3$/ CO_2/ H_20/N_2 (or parts of this system) which is considered a realistic model of the working industrial catalysts used for sulfuric acid production and removal of SO_2 from flue gas, For the first time, high temperature vibrational spectra have been obtained for the very dark, viscous and hydroscopic V_2O_5-$M_2S_2O_7$·M_2SO_4(M= alkali metal) melts and the spectra obtained are conclusively interpreted. A series of vanadium compounds in the oxidation state III, IV, V and of mixed valence V(IV)-V(V) have been isolated from catalyst model systems and characterized by thermal, spectroscopic and X-ray methods, These compounds are identified as catalyst deactivation products. Various physichochemical properties for the above complex molten salt-gas system (specific conductivities, heat capacities, vapor pressures etc.) have been established. Equilibrium vapor pressures over $KHSO_4$-$K_2S_2O_7$ and V_2O_5-$KHSO_4$-$K_2S_2O_7$ systems at 20-500°C were defined using the Boiling point method, the Quartz-Bourdon method and a newly developed vapor pressure measurement technique which can be used for measurements in the region from 10 torr to 10 bar. Two unique versatile apparatuses enabling combined catalytic activity measurements and real-time spectroscopic (ESR, UV-VIS) studies of commercial catalysts and catalyst model systems in SO_2 containing gases (or in any gas mixture) up to 1200 K have been constructed. The results obtained on SO_2 oxidation catalysts show good accordance between temperature of catalyst deactivation and the simultaneous precipitation of V(IV) or V(III) compound as detected by ESR. The complex and redox chemistry of vanadium in the catalyst solvent melt have also been investigated by means of spectroscopic and electrochemical methods at high temperatures. Furthermore, phase diagrams of the catalyst model systems $M_2S_2O_7$-V_2O_5 (M = Na, K, Cs) and $KHSO_4$-$K_2S_2O_7$ have been constructed, The results are considered useful for understanding the mechanism of $S0_2$ oxidation by alkali promoted V_2O_5 catalysts at the molecular level, for exploring the routes of catalyst deactivation experienced at temperatures below 400°C and for the design of modified catalysts with high activity also below 400 ‘C.

INTRODUCTION

The aim of the project is to obtain information on the fundamental chemistry of catalysts used for SO_2 oxidation in manufacturing of sulphuric acid and cleaning of industrial off-gases for SO_2. On this scientific basis the desired improvement of the activity of the catalysts below 400 °C might be achieved in a systematic, non-empirical way.

The typical catalyst composition is 6 wt. % V_2O_5 on kieselguhr promoted by alkali salts with an alkali to vanadium ratio in the range M/V = 2-4 (M = Na, K, Cs). In contact with the typical gases 10% SO_2, 11%02 and 79% N_2 (sulfuric acid production) or 0.2% SO_2, 4'% O_2, 7% H_2O, 14% CO_2 and 75% N_2 (power plant flue gas) SO_2 is converted to SO_3 and molten pyrosulfates and/or hydrogensulfates are formed in the pores of the industrial catalysts at 400 -500 °C. Thus the molten salt - gas system $M_2S_2O_7/MKHSO_4/V_2O_5$ - $SO_2/O_2/SO_3/CO_2/H_2O/N_2$ (or parts of this system) is considered a realistic model of the working industrial catalysts [1]. V_2O_5 dissolves in the pyrosulfate - hydrogen sulfate melt and forms complexes of V(V) [2] which are essentially the catalytically active species. In contact with SO_2 containing gases also V(IV) and V(III) complexes might be formed and at lower temperatures vanadium compounds of these low oxidation states may precipitate and deplete the catalyst for the active material.

Therefore a deep insight into the complex, redox and compound chemistry of vanadium in the catalyst is valuable for the understanding of the catalyst performance and for the systematic optimization of catalyst composition.

The hydroscopic, viscous and dark catalyst melts are very difficult to investigate at in situ conditions, i.e. at temperatures up to 500 °C and in contact with SO_2/SO_3 containing gases. A multiinstrumental research strategy has been applied involving combined spectroscopic, thermal, electrochemical and X-ray methods, whereby more reliable results can be obtained.

EXPERIMENTAL

Chemicals and samples' preparation.

The hydroscopic $K_2S_2O_7$ and $Cs_2S_2O_7$ used were obtained by thermal decomposition of $K_2S_2O_8$ and $Cs_2S_2O_8$ at 280-300°C in a stream of nitrogen and were stored in sealed ampules in the glove-box until use to avoid formation of hydrogen sulfate, as earlier described [2]. $K_2S_2O_8$ was from Merck (p.s.) while $Cs_2S_2O_8$ is not commercially available and it was synthesized as previously [3]. V_2O_5 (Cerac, Pure 99.9%), K_2SO_4 (Fluka) and Cs_2SO_4 (Fluka) were dried by heating *in vacuo* at 300°C for 4 hours and stored in the glove-box until use. The gases used were SO_2 (Matheson, Union-Carbide, 99.98%), N_2 (L'Air Liquide, 99.999%), O_2 (L'Air Liquide, 99. 99%) and SO_3 which was generated as described previously [4] by using a suitable flow control panel comprising thermal mass flowmeters (Brooks Modei 5850E) and a platinum-catalysed flow tank reactor operated at 380°C. Ail handling of the chemicals and filling of the various UV/VIS (Fig. 2), conductivity, ESR, Raman and reactor cells (Fig. 1) took place in nitrogen-filled glove-boxes (McBrown, Germany) with a measured water vapour content of below 5 ppm.

Catalysts

The commercial catalysts investigated were VK-WSA, VK38 and VK58 manufactured by Haldor Topsoe A/S, Denmark and a few from other important manufactures of the world.

The VK-WSA is applied in the flue gas desulfurization process and has the same chemical composition as VK38 (molar ratio K/Na/V=3/0.8/1, V_2O_5= 6.5 % w/w) but with a smaller average pore-size of the support. The VK58 catalyst has a modified chemical composition (molar ratio K/Cs/Na/V=3/1/0.25/1) including Cs in addition to K and Na as promoters. The catalyst pellets were crushed to a size of 1-1.5 mm and placed in the flow-reactor or in the high temperature ESR cavity cell, as earlier described [5].

Flue gas generation system

Feed gas with composition similar to dry flue gas (without NO_x) was prepared by mixing SO_2 (> 99.9%), O_2 (99.8% O_2, 0.2% Ar+N_2), CO_2 (> 99.7%) and N_2 (< 40 ppm H_2O+O_2) either by individual flowmeters or by premixing the gases in an evacuated special steel gas bottle followed by external heating at the bottom to obtain a uniform gas mixture by convection. A flow diagram is shown in Fig. 3. The absence of NO_x corresponds to the conditions of the SO_2 oxidation in the SNOX-process where NO_x is removed upstream [6]. The SO_2 concentration was monitored by UV-spectrophotometry on a Perkin Elmer Lambda-9 or a Hitachi U 3000 spectrophotometer, using a gas cuvette (quartz Suprasil, Hellma GmbH) with a path length of 100 mm, The concentrations of O_2, CO_2 and N_2 were checked by gas chromatography on a Shimadzu GC-8APT equipped with Supelco Chromosorb 102 or Molecular Sieve 5A columns.

Wetting of the flue gas was achieved by bubbling the dry gas until saturation through water which was contained in two flasks connected in series and immersed in a thermostat controlled at the appropriate temperature. With a thermostat temperature of 40 “C a 7% water vapour content was achieved. The water vapour concentration was measured by a Jenway 5075 Humidity meter. All 118” stainless steel tubes in the experimental set-up were heated to 80-90 °C by wrapped heating tape, in order to prevent condensation.

EPR and Catalytic Activity Set-up

For the activity measurements and compound isolation, the gases were led (Fig. 3) to a molten salt reactor of Pyrex. The reactor cell was mounted in a double walled canthal wire wound quartz tube furnace [4]. The temperature was controlled to within ± 2 °C and measured

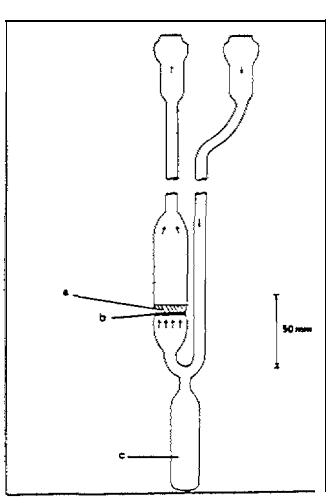

Figure 1. Molten salt reactor cell; a) catalyst melt, b) sintered glass filter disk, c) bottom ampoule for filtrate collection. Arrows indicate direction of flow during catalyst operation. The flow direction is reversed for filtering the” melts and isolating the crystalline precipitates

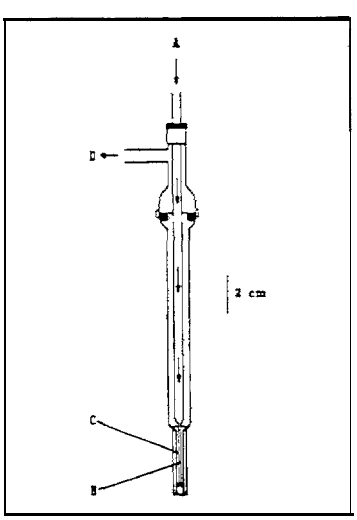

Figure 2: Gas - molten salt optical reactor cell. (A): gas inlet, (B): capillary tube immersed in the melt, (C): molten salt mixture, (D): gas outlet. The capillary tube was lifted above the melt surface during the measurements of the spectra.

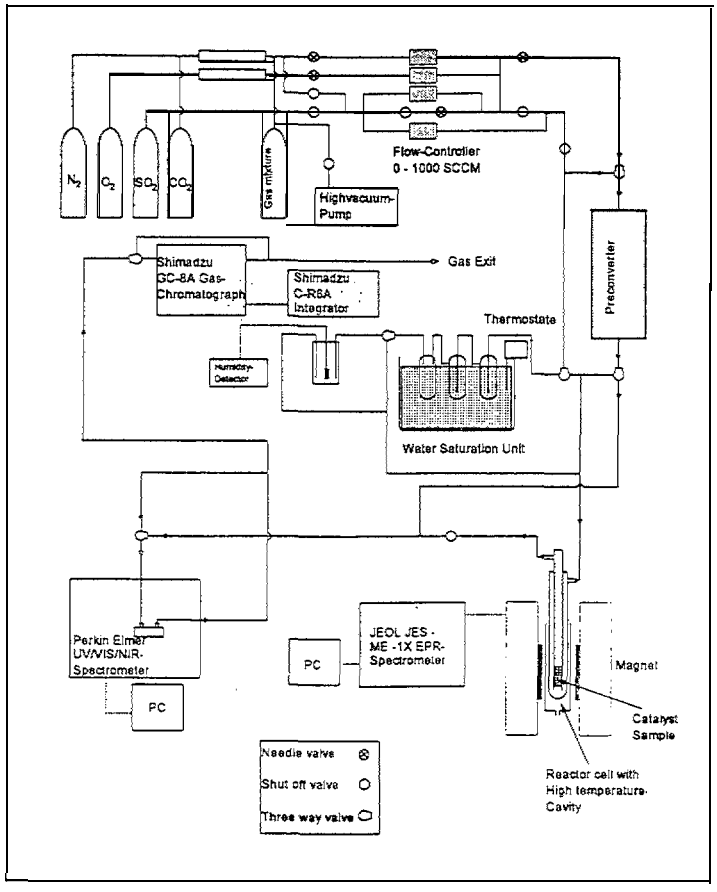

Figure 3. Set-up for in-situ catalysts' testing and characterization.

by a chromel-alumel thermocouple placed at the reactor cell area containing the catalyst sample. The reactor exit gas stream was passed through stainless steel tubes to a SO_3 trap made of borosilicate glass and placed in an antifreeze bath at -35 °C cooled by an immersion cooler before flowing to the spectrophotometer. Here the $S0_2$ conversion was monitored by on-line UV-spectrophotometry and the conversion was always below 15%. Thus the reactor could be considered as differential.

For the EPR-investigations, a set-up almost identical to that described above was used. Only the SO_3 cooling trap was replaced with an acid absorber of 98°/0 w/w sulfuric acid. The flue gas was led to a quartz reactor flow cell as described in detail earlier [5] which fits into a Bruker ER4114HT high temperature X-band cavity mounted in a slightly modified JEOL-JES-ME 1X EPR spectrometer connected to a PC-based acquisition system. The temperature was measured by a 1 mm non-magnetic chromel-constantan thermocouple placed in contact with the catalyst bed. The field calibration was performed with a external Mn(II)-standard and to correct the signal intensity for the temperature dependence, an internal separate ruby crystal was applied. The space velocity was adjusted in the range 5000-10000 h-' so the conversion over the catalyst bed was always below 15%.

Raman spectra

The samples were prepared by mixing V_2O_5 (Cerac, Pure 99.9%), $Cs_2S_2O_7$ and Cs_2SO_4 (Fluka) which was dried by heating *in vacuo* at 300°C for 4 hours. All handling of

chemicals and filling of the Raman optical cells [made of cylindrical fused silica tubing (4±0.1 mm o.d., 2±0.1 mm id. and ~3 cm long for the part containing the molten salts)] took place in a nitrogen-filled glove box. The samples were sealed under a low pressure (ea. 0.2 atm) of O_2 (L'Air Liquide, 99.99%) **in order to stabilise vanadium in the pentavaient state and** were **equilibrated at** 450°C **for up to 20 days before recording the** Raman spectra. This was necessary due to the slow dissolution of sulfate. Ram an spectra were excited with the 647.1 and 676.4 nm lines of a Spectra Physics Stabilite model 2017 krypton ion laser. The experimental set-up used and the procedures followed **for obtaining Raman spectra** at high temperatures **have been described in** *detail elsewhere*[7]. **it should be pointed out** here that recording of the Raman spectra at elevated temperatures from these very dark-coloured, viscous and hydroscopic melts has proven very difficult due to **strong absorption of** the incident exciting laser light.

RESULTS AND DISCUSSION

Vanadium (V) complexes in molten salts of interest for the catalytic oxidation of sulphur dioxide. A high temperature Raman study.

Several V_2O_5-$Cs_2S_2O_7$ mixtures with compositions $X^0_{V_2O_5}$= O -0.2 were placed in cells. Upon dissolution of V_2O_5 in the pyrosulfate solvent at 450°C, dark brown melts were obtained and Raman spectra could not be recorded for melts with $X^0_{V_2O_5}$>0.2 due to very strong absorption of the excitation laser lines used. Fig. 4 shows Raman spectra of V_2O_5-$Cs_2S_2O_7$ molten mixtures obtained at 450°C for four different compositions [Fig. 4(*b-e*)]. The Raman spectra of pure molten caesium pyrosulfate were also recorded and are included in Fig. 4(a) for comparison. The strongest band of the $S_2O_7^{2-}$ ion is at 1078 cm^{-1}. Addition of V_2O_5 gives rise to the appearance of several new bands [*i.e.* other than the ones due to $Cs_2S_2O_7$(l)]. The most prominent new features are at 1176, 1047 (due to 'V=O terminal stretching), 996, 839, 765, 670/690, 393, 302 and 205 cm^{-1} and are indicated in Fig. 4 by vertical lines. The existence of the 765 and 670/690 cm^{-1} bands is better illustrated in Fig. 4 (insert A) where the contribution **of** the 725 cm-l $S_2O_7^{2-}$ band is subtracted from the 600-1000 cm^{-1} region of spectrum (b). The intensities of all the above new bands increase relative to the bands of the $S_20,^{2-}$ ion with increasing $X^0_{V_2O_5}$ and dominate the spectrum (*e*) of the sample with $X^0_{V_2O_5}$=0. 2 indicating that the reaction taking place leads to a vanadium oxo sulfato complex at the expense of the $S_20,^{2-}$ ion. By plotting (see insert B, Fig.4) the quantity $[I(S_2O_7^{2-},1078)/X^0_{S_2O_7}]/[I(V=O,1047)/X^0_{V_2O_5}]$ VS. $X^0_{V_2O_5}$ - where $I(S_2O_7^{2-},1078)$ and I (V= O,1047) are the relative intensities due to $\nu_1(S_2O_7^{2-})$ and V=O in each composition and X^0_i are the initial moie fractions (weighed-in amounts) - it becomes evident by extrapolation that for $X^0_{V_2O_5}$=0.33 there would be no $S_2O_7^{2-}$ left. By taking into account the NMR[8] evidence suggesting the existence of *dimeric* V" *complex* furthermore strengthened by the fact that the only crystalline V" compound isolated so far from V_2O_5-$Cs_2S_2O_7$ molten mixtures is the $Cs_4(VO)_2O(SO_4)_4$[9], it follows that the reaction taking place can be formulated only **as** in eq (1)

$$V_2O_5 + 2S_2O_7^{2-} \cdot (VO)_2O(SO_4)_4^{4-} \qquad (1)$$

Within the $Cs_4(VO)_2O(SO_4)_4$ compound[9] there are four crystallographically different bidentate chelating significantly distorted sulfate groups with S-O bonds having largely varying distances, The terminal S-O bonds are in the range 1.43 -1.44Å while the S-() bonds involving oxygen coordinated to vanadium (bridging S-O bonds) are unusually long ranging between 1.52 and 1.58Å, far from the usual value of 1.47Å found for the ideai sulfate group. Furthermore, **a**

value of 961 cm-' is found for the $\nu_1(SO_4^{2-})$ mode of free sulfate in $Cs_2S_2O_7$-Cs_2SO_4 melts [see Fig.5(*a*)]. it is therefore evident that, if the $(VO)_2O(SO_4)_4^{4-}$ ion is the dimer complex formed in the molten state, then one could assign the 996 cm^{-1} band to the short terminai S-O stretching mode (S-O_t) and the 839 cm-' broad band to the long bridging S-O modes (S-O_b). The above variation in sulphur-oxygen stretching frequencies is compatible with the departures from the 1.47Å ideai S-O bond length and is analogous to the differences observed between terminal and bridging metal-halogen stretching frequencies [l O]. The 1176 cm-' band is identified as the $\nu_3(SO_4^{2-})$ mode. The 1047 cm^{-1} is assigned to the V^V=O terminal mode in agreement with what would be expected[10], while the 765 and 670/690 cm-' bands are assigned to V-O bridging. In particular, the 765 cm-' band is assigned to the V-O-V bridging mode of the dimer $(VO)_2O(SO_4)_4^{4-}$ complex and the 670/690 cm-' doublet band is due to V-O bridging involving sulfate oxygen (along the -V-U-S- chains). Such an assignment for these bands is in agreement with the relative V-O distances along the -V-O-S- and -V-O-V- chains within the $Cs_4(VO)_2O(SO_4)_4$ compound[9] and with a correlation between V-O Raman stretching frequencies and bond lengths[11].

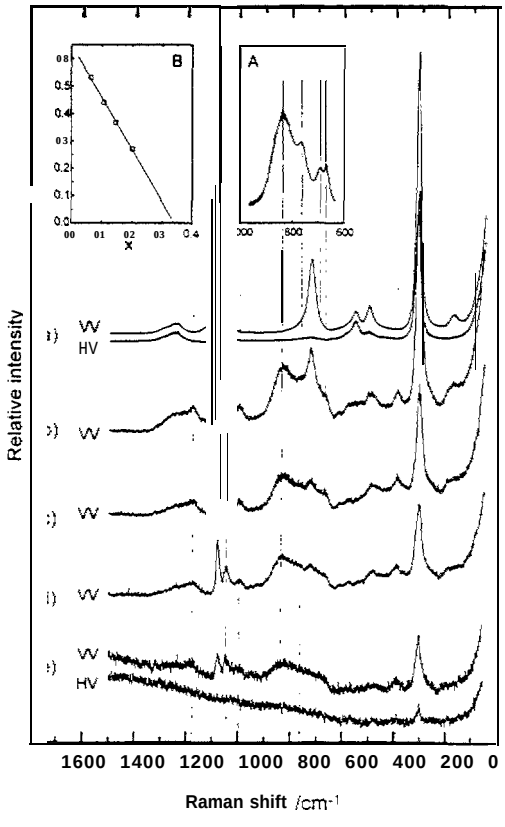

Figure 4: Raman spectra of the V_2O_5-$Cs_2S_2O_7$ molten mixtures at 450°C ; (*a*) $X^0V_2O_5$=0; (*b*) $X^0V_2O_5$ =0.065; (*c*) X $^0V_2O_5$:=0.106 (*d*) $X^0V_2O_5$ =0.146 and (*e*) $X^0V_2O_5$ =0.200. Bands due to the $(VO)_2O(SO_4)_4^{4-}$ (I) complex are marked by vertical lines. λ_0=647.1nm; laser power, w= 175 mW; scan rate, sr, 60 cm-' rein"' for (*a-d*), 18 cm"' rein" for [e); time constant, T, 0.3s for (*a*) , 1 s for (*b-d*), 3s for (e); spectral slit width, sw, 7 cm-'. VV and HV denote the vertical-vertical and horizontal-vertical spectra polarizations, respectively. Insert A: Region of spectrum (*b*) after subtraction of the 725 cm"' $S_2O_7^{2-}$ band. Insert B Plot of $I^*=[I(S_2O_7^{2-},1078)/X^0S_2O_7]/[I(V{=}O,1047)/X^0V_2O_5]$ vs. $x = X^0V_2O_5$ for the four compositions (*b-e*) studied (see text).

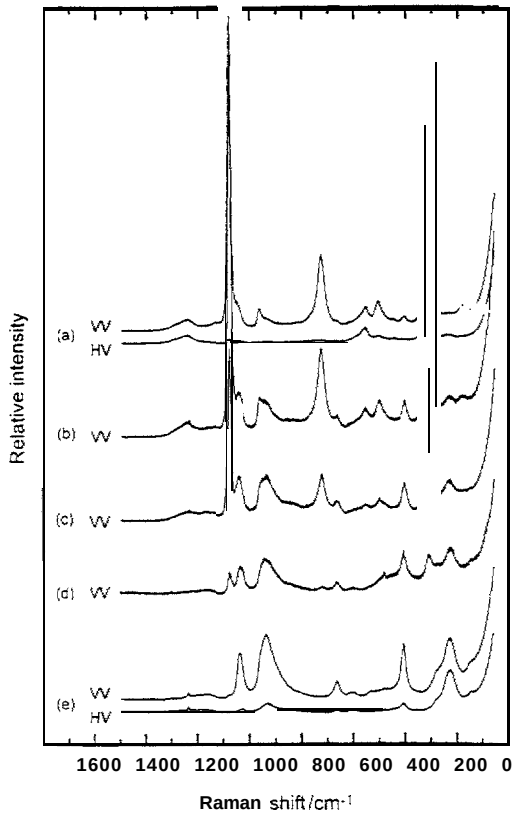

Figure 5: (A) Raman spectra of the V_2O_5-$Cs_2S_2O_7$ molten mixtures saturated with Cs_2SO_4 at 450°C ; $X^0V_2O_5$=0.027 (*a*); $X^0V_2O_5$ =0.066 (*b*); $X^0V_2O_5$ =0.147 (*c*) and $X^0V_2O_5$ =0.330 (*d*). $X^0V_2O_5$ is the mole fraction of V_2O_5 in the V_2O_5-$Cs_2S_2O_7$ mixture before addition of Cs_2SO_4. (B) Raman spectra of the V_2O_5·$Cs_2S_2O_7$·2Cs_2SO_4 molten mixture at 450°C [e). λ_0=647.1nm; laser power, w= 175 mW; scan rate, sr, 90 cm"' rein"' for (*a-c*), 30 cm" rein"' for (*d*), 60 cm^{-1} rein"' for (*e*); time constant, T, 0.3 s for (*a-c*) , 1s for (*d-e*); spectral slit width, sw, 7 cm"'.

Addition of Cs_2SO_4 to V_2O_5-$Cs_2S_2O_7$ melts results in reactions with the $(VO)_2O(SO_4)_4^{4-}$ complex, The reaction was followed by recording Raman spectra at 450°C for a V_2O_5-$Cs_2S_2O_7$ sample with fixed $X^0_{V_2O_5}$ in which various amounts of Cs_2SO_4 were added, A titration-like series of Raman spectra was thus obtained, which indicates that the V" dimer complex $[(VO)_2O(SO_4)_4^{4-}]$ reacts with the added sulfate up to a SO_4^{2-}/V^V ratio (ratio of number of added sulfate moles reacting vs number of extant V(V) atoms) equal to 1. Fig. 5(*a-c*) shows Raman spectra of V_2O_5-$Cs_2S_2O_7$ melts with $X^0_{V_2O_5}$ = 0.027-0.147 saturated with Cs_2SO_4. The band at 961 cm-l in spectrum 5(*a*) is due to the ν_1 mode of dissolved free SO_4^{2-}. The band at 941 cm-l is due to coordinated sulfate and its relative intensity increases with increasing content of V_2O_5 [see e.g. spectra (*b-c*)]. Furthermore, a comparison of spectrum 4(*d*) with 5(*c*) from samples with the same initial $X^0_{V_2O_5}$ = 0.15 shows that reaction with Cs_2SO_4 results in elimination of the 996 ($S\text{-}O_t$), 839($S\text{-}O_b$), 765 (V-O-V) and 302 cm-l bands, appearance of a new S-O stretching mode at 941 cm^{-1} and small shifts of the V^V=O to 1038, of the V-O-S to 666 and of the $\nu_3(SO_4^{2-})$ mode to 1166 cm^{-1}. Finally a low frequency doublet at 226/279 cm-l also appears. Thus, addition of Cs_2SO_4 results in cleavage of the V-O-V bridge and in formation of a V^v complex which contains slightly distorted coordinated sulfate groups.

The compound $Cs_4(VO)_2O(SO_4)_4$ was synthesised by fusing a V_2O_5-$Cs_2S_2O_7$ mixture with $X^0_{V_2O_5}$ = 0,33 ; it was afterwards mixed with excess Cs_2SO_4 and equilibrated at 450°C. The Raman spectrum of the resulting melt is depicted in Fig. 5 (*d*) and shows that the reaction proceeds with the formation of $S_2O_7^{2-}$ as indicated by 'the presence of the characteristic [see Fig.4(*a*)] 1078, 725 and 313 cm^{-1} bands. The above observations of i) a 1:1 SO_4^{2-}/V^V ratio of number of added sulfate moles reacting vs number of V^v atoms, ii} cleavage of the V-O-V bridge and production of $S_2O_7^{2-}$ upon sulfate addition are accounted for by the following reaction

$$(VO)_2O(SO_4)_4^{4-} + 2SO_4^{2-} \rightleftharpoons 2VO_2(SO_4)_2^{3-} + S_2O_7^{2-} \qquad (2)$$

Eqs (1) and (2) indicate that if all the hypotheses made up to now are correct, the constituents of a V_2O_5·$Cs_2S_2O_7$·$2Cs_2SO_4$ molten mixture would react at 450°C stoichiometrically to produce the $Cs_3VO_2(SO_4)_2$ molten complex without leaving excess solids or pyrosulfate ions, This is indeed the case as shown in Fig. 5(*e*). From a structural point of view, the $VO_2(SO_4)_2^{3-}$ complex can be formulated from the dioxovanadium ion and two bidentate chelating sulfate groups so as to satisfy the Preferential six-fold coordination for the vanadium atom and could occur as a monomer in dilute systems or as a $(VO_2(SO_4)_2)_n^{3n-}$ polymer in concentrated melts possessing one bidentate chelating and *one* bidentate bridging sulfate per monomer unit.

The results of the present communication concerning the formulae and the structural properties of the active V^v complexes are considered important for understanding the reaction mechanism of the SO_2 oxidation at the molecular level.

Degree-of-vanadium-reduction measurements and Temperature Dependence of Redox Equilibria

From the results of combined high temperature UV-VIS and ESR spectroscopic studies [12], it has become evident that the most plausible types of redox equilibria are the ones represented by eqs. (3-4)

Model "2" $\quad (V^V)_2 + SO_2 = 2V^{IV} + SO_3 \qquad (3)$

Model "3" $\quad 2V^V + SO_2 = 2V^{IV} + SO_3 \qquad (4)$

In Figure 6 all data for Models 2 and 3 obtained in the temperature range 430- 480°C are plotted and essentially linear dependencies are observed in all cases. From the slopes of the plots in Figure 6 the equilibrium constants for the two models were determined at the four measuring temperatures and plotted as lnK vs 1/T in Figure 7. The expressions for the redox equilibria according to models 2 and 3 shown in Figure 7 are suggested by following the general knowledge of the complex chemistry of V(V) in pyrosulfate melts and adopting the V(IV) configuration involving a VO^{2+} unit coordinated with two bidentate sulfate ligands discussed also above. The slopes of the plots shown in Figure 7 correspond to the enthalpies, ΔH^{ρ}, for the indicated equilibria as follows:

$$(VO)_2O(SO_4)_4^{4-}(l) + SO_2(g) \rightleftharpoons 2VO(SO_4)_2^{2-}(l) + SO_3(g) \qquad (5)$$

$$\Delta H^{\rho} = -107 \pm 4 \text{ kJ}^{-1}\text{mol}^{-1}$$

for Model 2 and,

$$2VO_2SO_4^{-}(l) + S_2O_7^{2-}(l) + SO_2(g) \rightleftharpoons 2VO(SO_4)_2^{2-}(l) + SO_3(g) \qquad (6a)$$

alternatively formulated as

$$2VO_2SO_4S_2O_7^{3-}(l) + SO_2(g) \rightleftharpoons 2VO(SO_4)_2^{2-}(l) + S_2O_7^{2-}(l) + SO_3(g) \qquad (6b)$$

$$\Delta H^{\rho} = -122 \pm 2 \text{ kJ}^{-1}\text{mol}^{-1}$$

for Model 3.

It has previously appeared impossible to distinguish between the two monomeric V(V) complexes participating in the redox equilibria (6a) and (6b). It should be pointed out that the concentration of $S_2O_7^{2-}$ has not been taken into account for the calculation of K_3. However, in 0,1 M V_2O_5 solutions in $K_2S_2O_7$, $[S_2O_7^{2-}]$ = 8.120 mol L"' at 450°C, as calculated from the densities of the V_2O_5 - $K_2S_2O_7$ system obtained previously. in the temperature range 435-

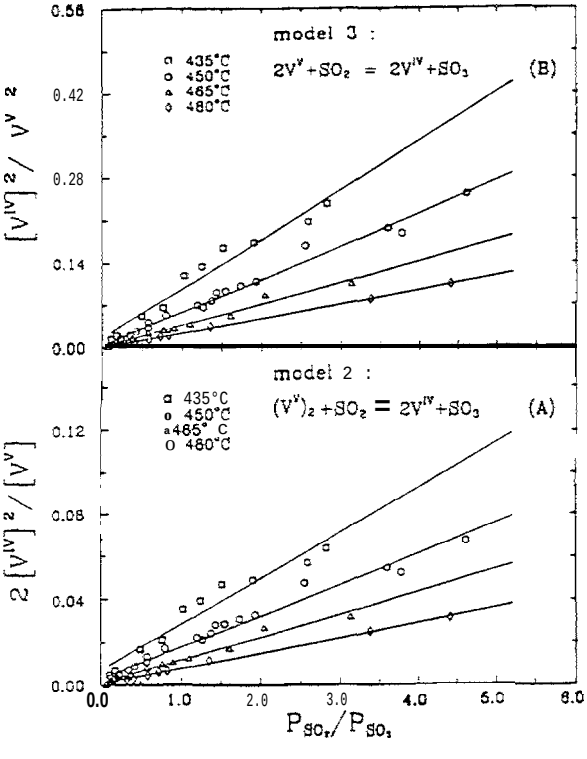

Figure 6. Plots of concentration quotients for models 2 and 3 vs P_{SO2}/P_{SO3} at 435 (□), 450 (○), 465 (Δ) and 480°C (◇). the data are obtained from a V_2O_5-$K_2S_2O_7$ mixture with C_0=0.1 **M** V_2O_5.

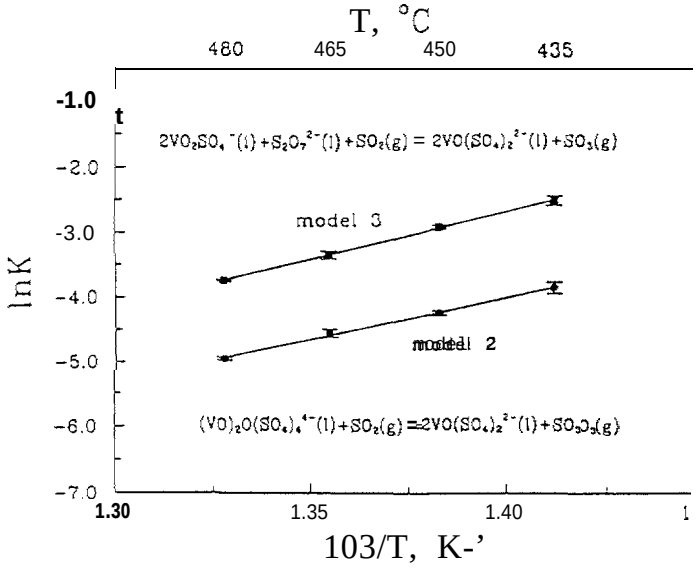

Figure 7. Plots of ln*K* vs 1/T for models 2 and 3. The concentration of $S_2O_7^{2-}$ has not been taken into account for the calculation of K_3

480°C investigated here, $[S_2O_7^{2-}]$ varies less than 1% from this value and accordingly it can be considered constant. Therefore the slope of the plot for Model 3 in Figure 7 and the enthalpy, ΔH^0, are not affected. It is noteworthy that the results from the high temperature Raman study point to a dimeric V(V) complex whereas previous cryoscopic measurements show that V(V) most probably is present as a monomeric complex in the concentration range of the present investigation. Thus, model 3 (e.g. expressed by equilibria (6a) and (6 b)) seems to be favored in dilute solutions.

Degree-o f-vanadium-reduc tion measurements. The redox equilibrium was studied at 450°C in molten V_2O_5-$K_2S_2O_7$ mixtures with initial concentrations CO (expressed in mol V_2O_5/L) in the range 0.1-0.5. These molten mixtures were equilibrated with gas atmospheres containing varying amounts of SO_2 and SO_3 (i.e. $P_{SO2} + P_{SO3} = 0.1$ atm, $P_{SO2} / P_{SO3} = 0.1 - 5$). The equilibrium concentrations of V(IV) and V(V) complexes were calculated and subsequently values-for the degree-of-vanadium-reduction ($[V^{IV}]/([V^{IV}]+[V^{V}])$ were determined. The results are displayed in Figure 8 and clearly indicate that the degree of reduction increases i) as the partial pressure of $S0_2$ and the ratio P_{SO2} / P_{SO3} are increased and ii) as the initial concentration of V_2O_5 is increased. Thus for example at 450°C and with P_{SO2}=0.06 atm (i.e. P_{SO3}=0.04) values of $[V^{IV}]/([V^{IV}]+[V^{V}]$ = 0.23, 0.35 and 0.55 are obtained **for melts with C_0 =** 0.1, 0.25 and 0.5 mol V_2O_5/L.

Temperature dependence of the degree-o f-vanadium-reduction. It has already been recognized how important the degree-of-vanadium-reduction is as a parameter. Often it is directly related to the catalytic activity for $S0_2$ oxidation since the stability of the V(V) complexes is the key factor for this process. H has also been observed during the catalytic activity measurements that a gradual decoloration of the melts occur as temperature is gradually lowered from 480°C to the region 400-420°C. Typically the melt color changes from dark brown to greenish-blue indicating an increased degree-of-vanadium-reduction. Figure 9 shows some very valuable Temperature dependence data that exhibit the strong influence of the temperature on the degree-of-vanadium-reduction. Thus, for example for a melt with Co = 0.1 mol V_2O_5/L and with P_{SO2}= 0.06 atm, i.e. P_{SO3}= 0.04 atm, values of $[V(IV)]/[V_{total}]$= 0.15, 0.17, 0.23 and 0.27 are obtained at temperatures 480, 465, 450 and 435*C, *respectively*.

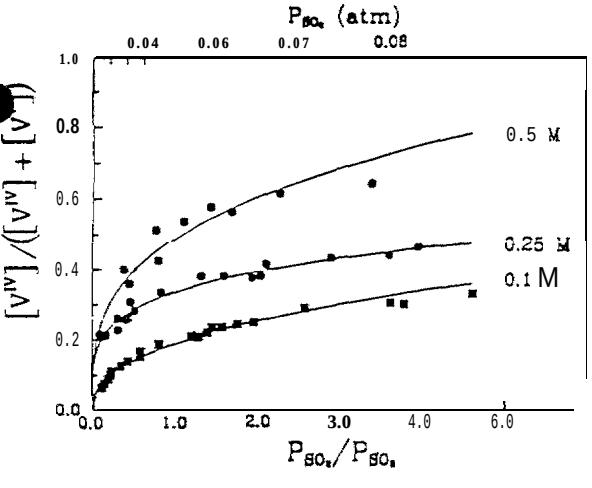

Figure 8. **Plot of the degree of vanadium reduction $[V(IV)]/[V_{total}]$ as a function of the partial pressure ratio of SO_2 and $S0_3$ (P_{SO2}/P_{SO3}) for V_2O_5-$K_2S_2O_7$ melts with initial concentrations C_0= 0.1, 0.25 and 0.5 mol V_2O_5/L at 450°C.**

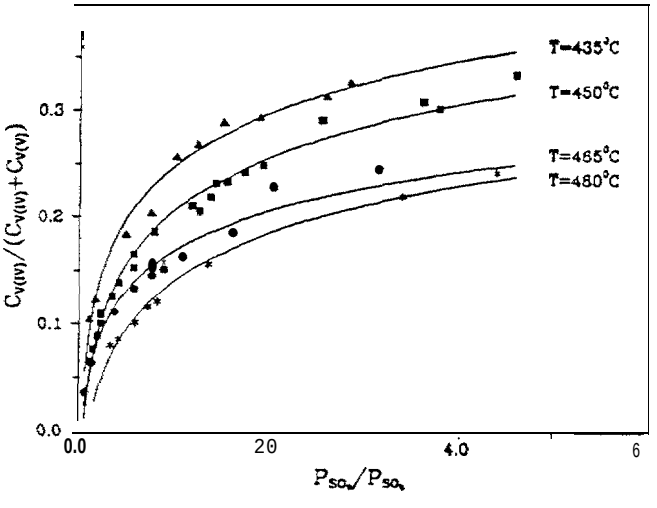

Figure 9 Temperature dependence measurements of the degree-of-vanadium-reduction ($[V(IV)]/[V_{total}]$) as a function of the partial pressure ratio of SO_2 and $S0_3$ (P_{SO2}/P_{SO3}) for V_2O_5-$K_2S_2O_7$ melts with initial concentrations C_0= 0.1 mol V_2O_5 /L

Vapor pressure measurements in the $KHSO_4$-$K_2S_2O_7$ and V_2O_5-$KHSO_4$-$K_2S_2O_7$ systems

The new vapor pressure technique was developed as a combination of the direct equilibrium vapor pressure measurement and Boiling-Point-Method, and can be used for measurements in the region from 10 torr to 10 bar at temperatures up to 500°C (Fig. 10).

The vapor pressure - temperature plots obtained by the new technique for pure $KHSO_4$ and the equimolar mixture of $KHSO_4$ and $K_2S_2O_7$ are given in Figs. 11 and 12. It can be seen . that the new technique gives the same results as the Quartz-Bourdon method and therefore both measurements are reliable. For both electrolytes the lnP vs. 1/T plots are linear as predicted by thermodynamics. The vapor pressure values for pure $KHSO_4$ are much higher than predicted by published data, reaching 8 bar at 500°C. It was defined that vapor pressure values over 10 mol% $KHSO_4$-$K_2S_2O_7$ are lower than 60 torr at temperatures up to 440°C and therefore this water concentration can be reached under the conditions for the industrial process. It can be concluded from Fig. 13 that in the presence of V_2O_5 (10 mol% V_2O_5 in equimolar $KHSO_4$-$K_2S_2O_7$) water vapor pressure is noticeably lower than for the $KHSO_4$-$K_2S_2O_7$ mixture. This was explained by complex formation between vanadium species and water molecules.

Electrochemical Investigation of the structure Of vanadium complexes and the vanadium reduction mechanism in V_2O_5-$M_2S_2O_7$ (M = K, Na, Cs or Li) and V_2O_5-$KHSO_4$-$K_2S_2O_7$ melts

The electrochemical behavior of V_2O_5 was studied in V_2O_5-$M_2S_2O_7$ (M= K, Cs, Na or Li) and V_2O_5-$KHSO_4$-$K_2S_2O_7$ melts at 440°C in argon, air and SO_2/air atmospheres [13] by means of cyclic voltametry, chronoamperometry and chronopotentiometry.

It was shown that all stages of the catalytic process can be reproduced electrochemically. V_2O_5 can be electrochemically reduced to V(III) compounds in two stages: V(V) → V(IV) (waves I-I and F in Figs. 14, 15) and V(IV) → V(III) (wave G in Fig. 14). Both V_2O_5 reduction stages are electrochemically irreversible, therefore they could be driven electrochemically. It was shown that H^+ reduction took place at 0.26 V vs. a Ag^+/Ag reference electrode (300 mV/s), i.e. at a potential in between the V(V) - V(IV) and V(IV) → V(III) reduction stages.

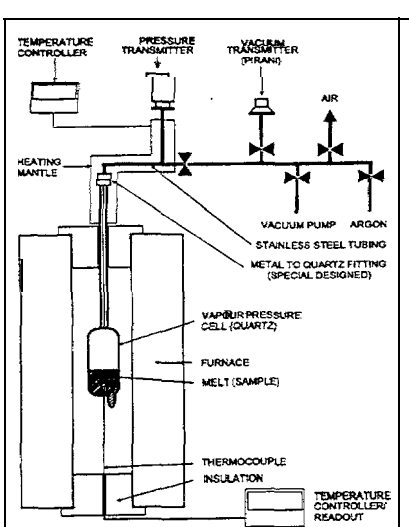

Figure 10. Diagram of the set-up for . new vapor pressure technique

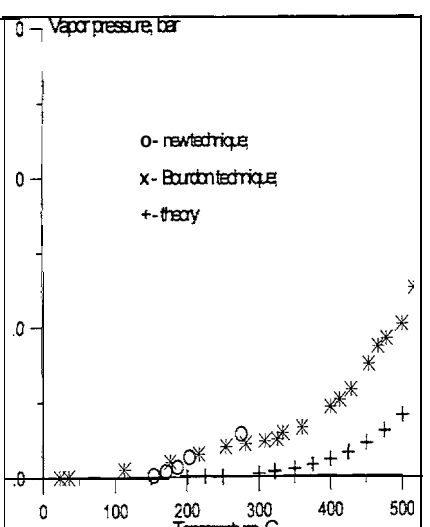

Figure 11. Equilibrium vapor pressure vs. temperature over 50 mol% KHSOt-50 mol% $K_2S_2O_7$

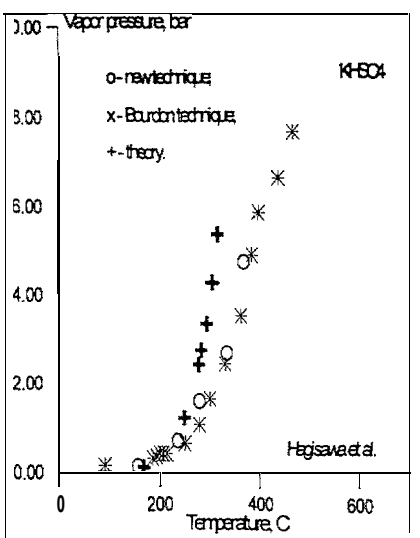

Figure 12. Equilibrium vapor pressure vs. temperature over $KHSO_4$

It can be seen that in the presence of $KHSO_4$, V(V) → V(IV) electrooxidation proceeds with higher polarization (Fig. 15) which is caused by the slow kinetics of this electrochemical reaction: linear E_p-lnV dependence shows the. irreversibility of the electron transfer stage.

The results of the voltammetric investigation in "dry" $K_2S_2O_7$-V_2O_5 (10 mol %) melt under the SO_2/air atmosphere show that the kinetics of the V(V) → V(IV) and V(IV) → V(V) reactions change from irreversible kinetics to kinetics with slow preceding chemical reaction. The only explanation can be a new structure of the active V(V) and V(IV) particles in the SO_2/air atmosphere. The diffusion coefficients for the V(V) particles were calculated from the $I\text{-}t^{-1/2}$ slopes using the Cottrel's equation. Change of the value of the diffusion coefficient in the SO_2/air atmosphere indicates change in the V(V) complex structure. Moreover lower values of diffusion coefficient can be caused by bigger size (cluster structure) of the vanadium particles. The results of the voltammetric study of V_2O_5-$KHSO_4$-$K_2S_2O_7$ melts under SO_2/O_2 atmosphere indicate that the water inhibition effect is still found for the V(IV) → V(V) oxidation, and that water has no (or even slight positive) effect on the V(V) → V(IV) reduction. Therefore the participation of water in both V(V) and V(IV) complexes can be assumed.

Cesium and sodium ions accelerate both the electrochemical V(V) → V(IV) reduction and V(IV) → V(V) oxidation stages, the Na^+ effect being more pronounced in the oxidation stage. In the presence of Cs^+ the rate of V(V) → (V(IV) is ca. 60% higher than in molten $K_2S_2O_7$-V_2O_5. In both argon and air atmospheres the highest promotion effect was for 7.5-8.5 mol% of $Na_2S_2O_7$ in molten $K_2S_2O_7$-V_2O_5 and ca 3% $Na_2S_2O_7$ in molten $Cs_2S_2O_7$-$K_2S_2O_7$-V_2O_5.

In situ ESR and activity measurements

The SO_2 oxidation catalysts VK38, VK58 and VK-WSA from Haldor Topsoe A/S as well as industrial catalysts from other producers and various unsupported molten salt mixtures have been investigated [14, 15, 16] by use of the catalyst test apparatuses described in the previous section. For convenience only selected results of the activity measurements will be shown.

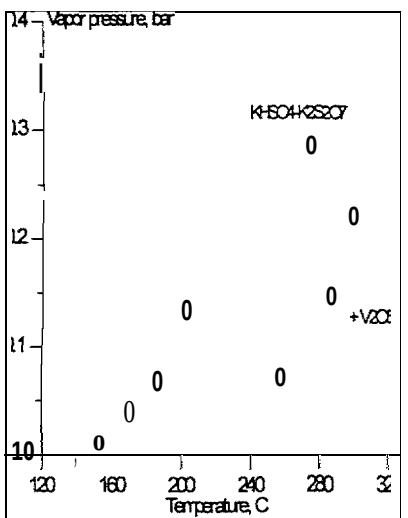

Figure 13. Vapor pressure vs. temperatuire over 50°% $KHSO_4$-50 mol% $K_2S_2O_7$ and 50% $KHSO_4$-50 mol% $K_2S_2O_7$ with 10% V_2O_5 obtained by the new technique

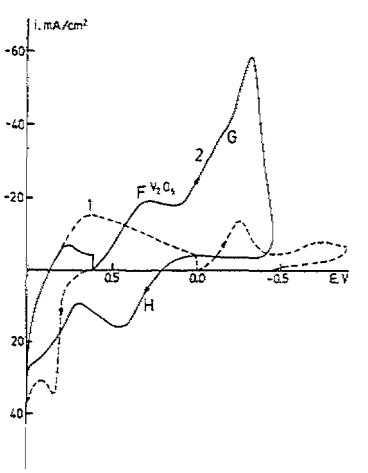

Figure 14. Cyclic voltammograms for (1) $K_2S_2O_7$ and (2) $K_2S_2O_7$ + 2 mol% V_2O_5 at 440 C and 0.1 V/S

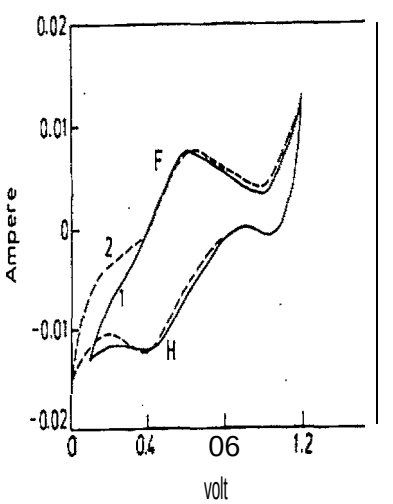

Figure 15. Cyclic voltammograms for $K_2S_2O_7$-10%V_2O_5 (1) and $K_2S_2O_7$- 10%V_2O_5-10 mol% $KHSO_4$ (2) at 100 mV/s and 440 C.

Catalytic ***activity of catalysts*** *and model melts in sulphuric acid production* ***synthesis gas.*** The catalytic activities of industrial catalysts and $M_2S_2O_7$-V_2O_5 model melts containing the various alkali promoters (M = Na, K, Cs) with M/V molar ratios between 3 and 10 have been measured in the temperature range 360-480 "C. A 5% SO_2, 5% SO_3, 9% O_2, 81% N_2, mixture was used as the feed gas, i.e. corresponding to 50% conversion of the IO*A SO_2, 11% O_2, 79% N_2 starting feed gas. Thus the measurements reflected conditions similar to those of the second catalyst bed. These results are displayed in Figure 16. Figures 17 and 18 illustrate the case for the industrial catalysts studied. All plots invariably exhibit a sharp break at a temperature T_b given in Table 1. In the high temperature region ($T>T_b$) the catalyst model systems are liquid, while formation of crystalline solids occurs below T_b. As temperature is gradually reduced, increasing amounts of precipitates are accumulated, Blue V(IV) and green V(III) salts were isolated from the melts either by filtration at high temperatures or by washing the solidified melts after cooling. In this way a whole series of low soluble V(IV) and V(III) compounds were isolated and characterized. Thus at temperatures below T_b the liquid phase of the catalyst is gradually depleted for active dissolved vanadium species.

The results of the investigation are summarized in Table L The apparent activation energies are comparable for the two different gas compositions. However, the break in these plots is shifted to **lower temperatures for** the melts **in the 500/. preconcerted gas.** This **is** probably **due to a shift of the formal equilibria system** (Eq.7) to **the**

$$V(V) \underset{SO_3}{\overset{SO_2}{\rightleftharpoons}} V(IV) \underset{SO_2}{\overset{SO_3}{\rightleftharpoons}} V(III) \qquad (7)$$

left, since the partial pressure ratio P_{SO3}/P_{SO2} is larger compared to the unconverted feed gas.

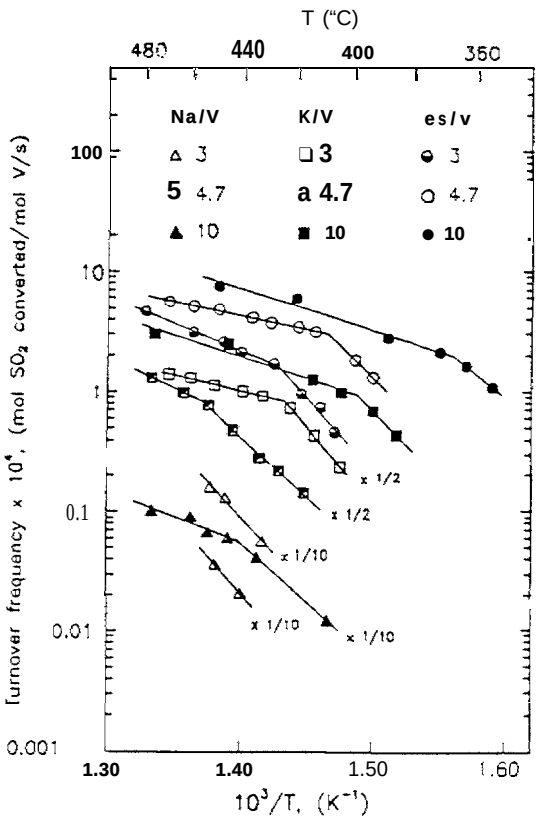

Figure 16. Arrhenius plots of the measured reaction rates for Na, K and Cs promoted catalyst melts. Feed gas 5% SO_2, 5% SO_3, 9% O_2, 81% N_2.

Thus the critical concentration (the volubility limit) of V(IV) and V(III) is achieved at lower temperatures in the 50[a]/o preconcerted gas and T_b is accordingly lower. Indeed recent spectrophotometric and ESR **measurements on dilute solutions** of V_2O_5 in molten pyrosulfates show that the V{ V)-V(IV) **redox equilibrium** is **shifted towards** V(IV) by lowering the temperature. Also the type of alkali promoter seems to influence the position of the **redox equilibria.** Thus it is known that increasing the radius of the alkali metal ion, i.e. in the sequence **Li, Na, K,** Rb, Cs, **increases the ability** of **their** sulphates **to absorb** SO_3 **(forming** pyro-sulphate **and higher** pyrosulfates) **and stabilize the vanadium** in **the** +5 **oxidation state. This trend is in accordance with the observed decrease of T_b for the** Na, K **and** Cs **based** model **melts, respectively with the** same **molar** ratio M/V **(Table l), but other factors, e.g.**

differences in the solubility product of the precipitating salts may also be significant. In the case of supported catalysts also the pore size distribution has significant influence. Furthermore, from Figure 16 and Table I it is seen that an increase of the MN ratio in the row 3, 4.7 to 10 leads in all cases to a decrease of T_b. This is presumably due to a simple dilution effect but probably also due to an increasing activity of $S_2O_7^{2-}$ in the melts through this row, shifting the redox equilibria towards V(V).

Table L Temperature of the Activity Drop and Apparent Activation Energies of the Catalyst Melts [a]

Model Melt or Catalyst	T_b [b] (°C)		Apparent activation energy (kcal/mol)			
	x_p=0	x_p=0.5	x_p=0		x_p=0.5	
	T_b	T_b	$T>T_b$	$T<T_b$	$T>T_b$	$T<T_b$
NaN=3	(>470)[c]	(>475)[c]		49.2		57.0
Na/V=4.7	(>460)[c]	(>460)[c]		49.2		54..5
Na/V=10	(>460)[c]	442		55.0	19.0	45.0
K/V=3	(>475)[c]	454		47.0	23.5	46.3
K/V=4.7	439	425	17.6	49.2	12.0	58,0
K/V=10	404	399	15.4	47,6	16.3	49.0
Cs/V=3	430	427	17.8	41.4	20.6	55.0
Cs/V=4.7	416	409	16.0	42.1	11.0	48.4
Cs/V=10	388	368	14.6	40,9	16.0	40.6
K/Na/V=3.7/1/1	432		18.1	46.3		
K/Cs/V=3.7/1/1	427		18.1	50.4		
K/Na/Cs/V=3.7/ 0.5/0.5/1	424		17.8	48.2		
Cs/K/V=3.7/1/1	412		19.3	45.2		
Cs/Na/V=3.7/1/1	407		17,2	45.4		
Cs/K/Na/V=3.7/ 0.510.5/1	390		17.2	43.4		
K/Na/V=3/0.8/1	454		18.5	34.6		
VK 38	441	431	18.6	35.6	1S3.2	43.8
VK 58	420	416	13.0	61.6	17.0	60.9
CING cat	437'		18.9	65.4		

[a] Feed gas composition: x_p=0, 100/0 SO_2, 11?400$_2$, 79°A I_2
x_p=0.5, 50/0 SO_2, 5% SO_3, 9'%00$_2$, 81% N_2

[b] T_b is the temperature at which the compound precipitation and the break in the Arrhenius plots occur simultaneously.

[c] T_b is above the highest measured temperature given in parentheses.

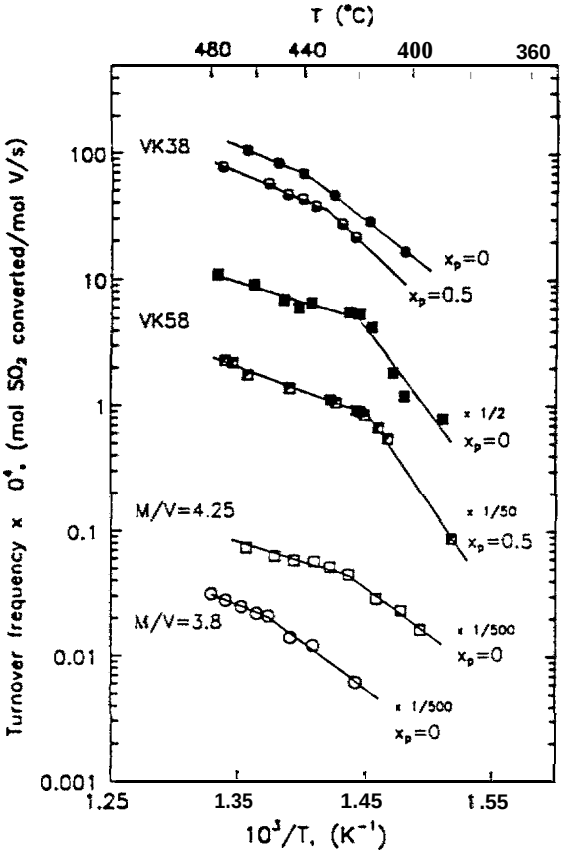

Figure 17. Arrhenius plots of measured reaction rates for the mixed-alkali promoted industrial catalysts VK-38, VK-58 (Na, K, Cs) and their model melts (K/Na/V = 3/0.8/1and K/Cs/Na/V=3/1/0.25 respectively). Feed gases: 10% S 0_2,11% 0_2, 79%.& (x_p=0) and 5% SO_2, 5% S 0_3, 9% O_2, 81% N_2(x_p=0.5).

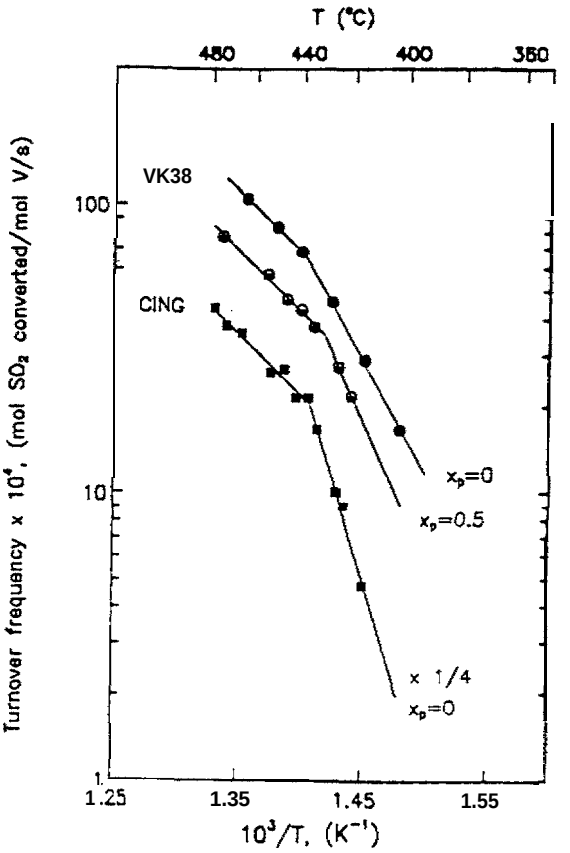

Figure 18. Arrhenius plots of the measured reaction rates for the VK38(Topsoe) and CING catalysts. Feed gases: 10% SO_2,11% 0_2, 79% N_2(x_p=0) and 5% SO_2, 5% SO_3, 9% O_2, 81% N_2 (x_p=0.5).

Industrial **catalysts** *in "wet" and "dry" flue gases.* **The catalytic activity - given as turnover frequency of** SO_2 **- (see Fig.** 19) **shows a sharp break by lowering** of **the temperature and below this temperature catalyst deactivation takes** place. **The breakpoint temperature (TJ exhibits a marked** change **towards lower temperature for the WK-WSA catalyst in "wet" (B} compared to "dry" flue gas** (A) **while** T_b **changes** only **slightly for the other catalysts. Obviously** the **much smaller pores of the** VK-WSA **carrier** is **responsible for this** behaviour **leading to suppression of the formation of solid** V(IV) **compounds whereby the volubility limit will be reached at a lower temperature** [15].

The ESR spectra shown in Figure 20 for the VK-WSA in **"dry"** (A) **and "wet"** (B) **flue** gas **are very different. In** "dry" **gas** the **break on the** plot **of apparent** line **width and the ESR parameters found at** the **lowest temperature indicate that the** V(IV) **compound [17]** $K_4(VO)_3(SO_4)_5$ **starts to precipitate at 408** °C **- close to the deactivation temperature found in Figure 19. However,** in **"wet" gas** no **break is found on the** ΔB_{pp} **vs** T **plot. Most likely an** ESR silent V(III) **compound** precipitates *in* **this case at** the **breakpoint temperature** *found in* **Figure 19. It could very well be** $KV(SO_4)_2$ **which earlier [18] has been isolated and characterized by us, This interpretation that catalyst deactivation is caused by precipitation is supported** by **the** hystresis **phenomena observed** [19] **for the activity during cooling and reheating, As an example this is shown on Figure 21 for** VK-WSA **in "wet" flue gas.**

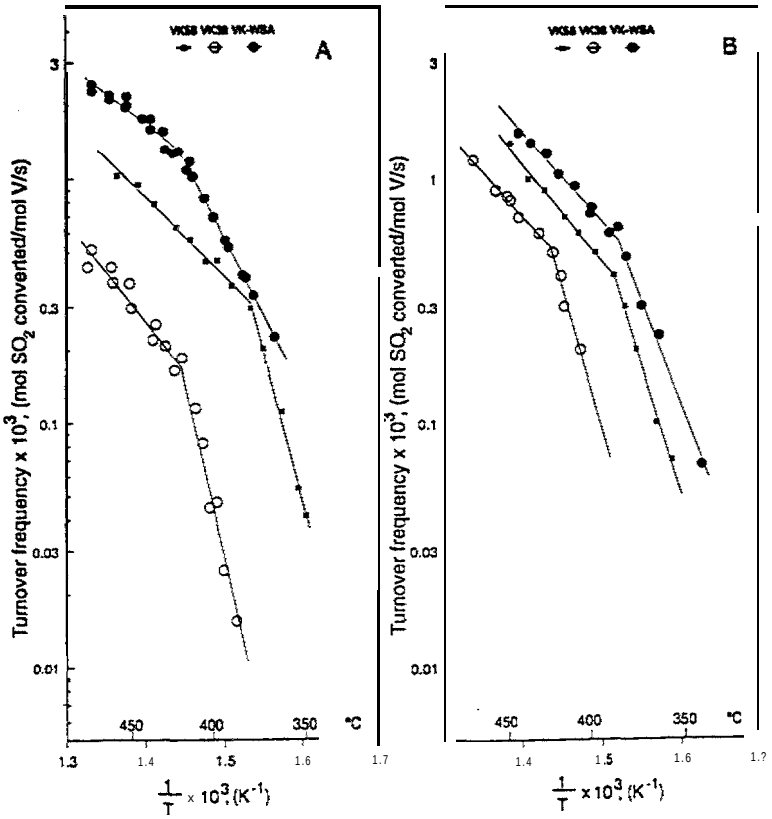

Figure 19. Arrhenius plots of the industrial catalysts VK38, VK58 and VK-WSA

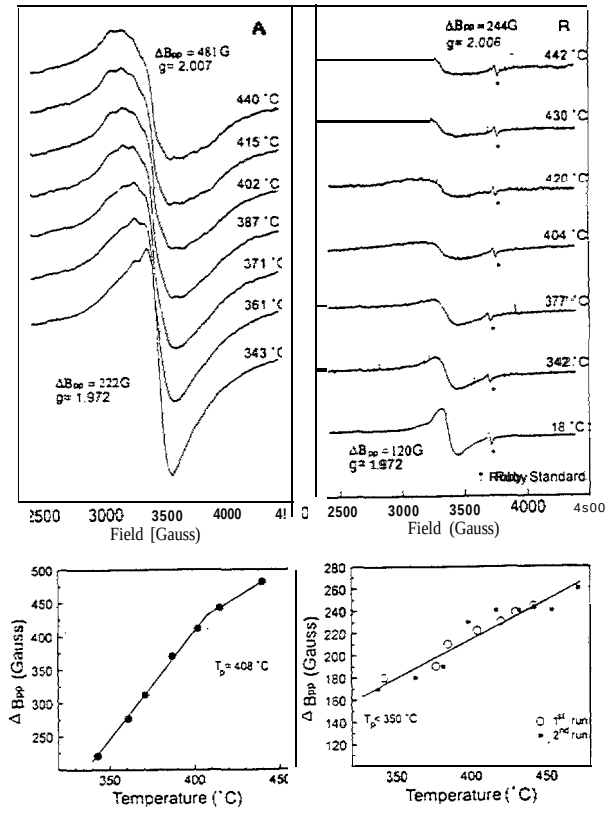

Figure 20. ESR spectra of VK-WSA in "dry" (A) and "wet" [B) flue gas

Table II. Compounds identified as catalyst deactivation products - compounds responsible for catalyst deactivation

V(IV)	V(III)
$Na_2VO(SO_4)_2$	$NaV(SO_4)_2$
	$Na_3V(SO_4)_3$
$Na_8(VO)_2(SO_4)_6$	
$K_4(VO)_3(SO_4)_5$	$KV(SO_4)_2$
$K_3(VO)_2(SO_4)_4$[a]	
$Cs_2(VO)_2(SO_4)_3$	$CsV(SO_4)_2$
β-$VOSO_4$	
$(VOSO_4)(SO_2SO_3)_x$	

[a] Mixed valence compound V(IV)-V(V)

During cooling the V(III) compound precipitates and reduces the concentration of active vanadium species in the catalyst melt. The compound is probably partly isolated in the pores of the carrier in bad contact with the residual melt. Thus the catalyst activity is lower on reheating until the temperature is reached where the compound decomposes and melts [4,14] leading to restoration of the full catalytic acitivity.

Isolation of solid compounds responsible for catalyst deactivation

The special design of the reactor cell (see Figure 1) enables the isolation of the crystalline compounds that are formed during the deactivation of the catalyst *under* ***operating*** *conditions*. Compound isolation is performed by *in-situ* filtration during activity tests of catalyst model melts right after the deactivation sets in, *i.e.* at a temperature slightly lower than the temperature of deactivation, T_b. The isolated crystalline vanadium compounds are characterized by X-ray, spectroscopic (IR, Raman, ESR) and thermal methods. Table II lists the 'crystalline compounds that are possibly responsible for catalyst deactivation.

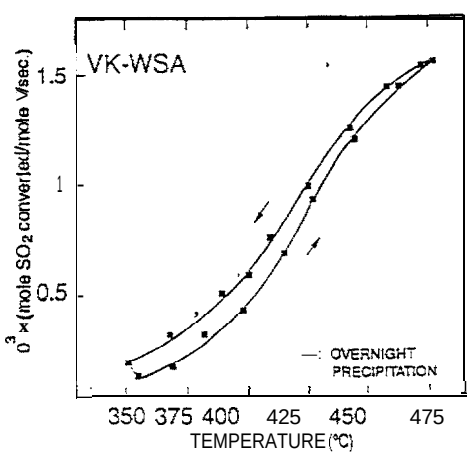

Figure 21. **Activity for VK-WSA during cooling and reheating**

Cs-promoted catalyst model melts

Most industrial catalysts are promoted by a mixture of K and Na. **However, Cs has** proven to enhance the activity below 400 °C as demonstrated for the Topsoe catalyst VK58, which contains around 25% Cs and 75% K + Na. Therefore the complex and compound chemistry **of** the $Cs_2S_2O_7$-V_2O_5 system is important to study. Thus the $Cs_2S_2O_7$-V_2O_7 phase diagram has been constructed [3] from thermal and electrochemical measurements and it was found that two compounds are found. One of them, the dimeric compound $Cs_2(VO)_2O(SO_4)_4$, is formed in the catalytic relevant composition range. High temperature NMR spectroscopy has revealed [8] that also for the composition Cs/V = 4 the dimeric species $(VO)_2O(SO_4)_4^{4-}$ seem to dominate in the solution, as judged from the ^{51}V NMR spectra in agreement with the results of the high temperature Raman study (see above). Thus the suggested [3] dimeric key complex for the catalytic conversion might be formulated as $(VO)_2O(SO_4)_4^{4-}$.

Phase diagrams of the $M_2S_2O_7$-V_2O_5 systems

Besides the above **mentioned phase diagram** of the $Cs_2S_2O_7$-V_2O_5 system [3], **other binary or pseudobinary catalyst** model **systems like** $K_2S_2O_7$-V_2O_5 [20], $Rb_2S_2O_7$-V_2O_5 [21] and $M_2S_2O_7$-V_2O_5 (M = 20% Na + 80% K) [22] have been investigated by combination of high temperature NMR spectroscopy or thermal analysis and conductometric measurements. As an example the phase diagram of the latter **is shown in Figure 22.**

This diagram exhibits the same features as the other investigated systems i.e. *one* **compound is formed around** $X_{V_2O_5}$ = 0.3 **and probably another at** $X_{V_2O_5}$ = 0.5 **and** two eutectics. However, **in** the $K_2S_2O_7$-V_2O_5 **system very recent** NMR measurements **has" revealed that a third compound seems to be formed at** $X_{V_2O_5}$ = **0.25. The compounds can probably** be formulated **as** $M_3VO_2SO_4S_2O_7$, $M_4(VO)_2O(SO_4)_4$ and MVO_2SO_4. Knowledge of the diagrams and **compounds seems useful for the design of low melting** catalysts.

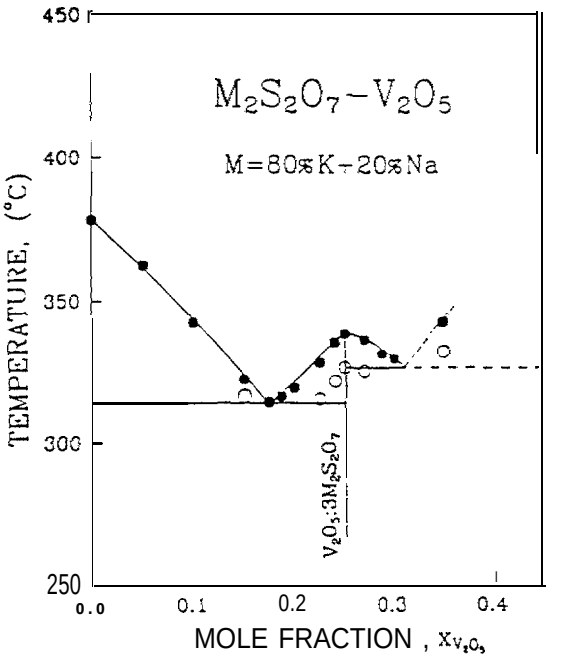

Figure 22. Phase diagram of the $M_2S_2O_7$-V_2O_5 (M= 20% Na + 80% K) system

ACKNOWLEDGMENTS

This work has been supported **by** the BRITE-EURAM Programme of the Commission of the European Communities (Contract BRE2.CT93.0447, Proposal PE-5020)

REFERENCES

1. J. Villadsen and H. Livbjerg, Catal. Rev. -Sci. Eng., 17 (1978) 203.
2. N.H. Hansen, R. Fehrmann and N.J. Bjerrum, Inorg Chem., **21 (1982) 1497.**
3. G.E. Foikmann, G. Hatem, **R.** Fehrmann, M. **Gaune-Escard and** N.J. Bjerrum, Inorg. Chem., 30 (1991) 4057.
4 S. Boghosian, R. Fehrmann, N.J. Bjerrum and G.N. Papatheodorou, J. Catal., 119 (1989) 121.
5. K.M. Eriksen, R. Fehrmann and N.J. Bjerrum, J. Catal., 131 (1991) 263.
6. D.J. Smith, Power Eng. Int., April (1994) 21.
7. S. Boghosian and G. N. Papatheodorou, J. Phys. Chem., 93 (1989) 415 and references therein.
8. O.B. Lapina, V.M. Mastikhin, K.M. Eriksen and R. Fehrmann, J. Molec. Catal. A,, 99 (1995) 123.
9. K. Nielsen, R. Fehrmann and K. M. Eriksen, Inorg. Chem., 32 (1993) 4825.
10. K. Nakamoto, *Infrared and Raman Spectra of Inorganic and Coordination Compounds,* Wiley-Interscience, New York, 1986, p. 140, 329,
11, F. D. Hardcastle and I E. Wachs, J. Phys. Chem., 95 (1991) 5031.
12. D. A, Karydis, K. M. Eriksen, R. Fehrmann and S. Boghosian, J. Chem. Sot, Dalton Trans., (1994) 2151.
13. N. J. Bjerrum, I. Petrushina and R. W. Berg, J. Electrochem. Sot., 142 (1995} 1806.
14. K.M. Eriksen, D.A. Karydis, S. Boghosian and R. Fehrmann, J. Catal., 155 (1995) 32,
15. C. Oehlers, R. Fehrmann, S.G. Masters, K.M. Eriksen, D.E. Shenin, B.S. Bal'zhinimaev and V.I. Elokhin, Appl. Catal., xxx (1996) in press,
16. S.G. Masters, A. Chrissanthopoulis, K.M. Eriksen, S. Boghosian and R. Fehrmann, J. Cabal., xxx (1996) accepted.
17, R. Fehrmann, S. Boghosian, G.N. Papatheodorou, K. Nielsen, R.W. Berg and N.J. Bjerrum, Inorg. Chem., 28 (1989) 1847.
18. R. Fehrmann, B. Krebs, G.N. Papatheodorou, R.W. Berg and N.J. Bjerrum, Inorg. Chem., 2.5 (1986) 1571.
19. S.G. Masters, K.M. Eriksen and R. Fehrmann, J. Molec. Catal., submitted.
20. S.G. Masters, C. Oehlers, K. Nielsen, K.M. Eriksen, R. Fehrmann, A. Chrissantopoulos and S. Boghosian, in *Molten Salts X,* R. Calin, S. Deki, M. Matsunaga, D. Newman, J. F?. Selman and G. Stafford Eds., The Electrochemical Society Proceeding Series, PV 96-7 (1996) 74.
21, F. Abdoun, R Fehrmann, K.M. Eriksen and G. Hatem, in prep.
22. D.A. Karydis, S. Boghosian and R. Fehrmann, J. Catal., 145 (1994) 312.